## MATERIALS SCIENCE

# Molecular origin of the two-step mechanism of gellan aggregation

**Letizia Tavagnacco**[1]*, **Ester Chiessi**[2], **Leonardo Severini**[2], **Silvia Franco**[1], **Elena Buratti**[1,3], **Angela Capocefalo**[1], **Francesco Brasili**[1], **Adriano Mosca Conte**[1], **Mauro Missori**[1], **Roberta Angelini**[1], **Simona Sennato**[1], **Claudia Mazzuca**[2], **Emanuela Zaccarelli**[1]*

Among hydrocolloids, gellan is one of the most studied polysaccharides due to its ability to form mechanically stable gels. Despite its long-standing use, the gellan aggregation mechanism is still not understood because of the lack of atomistic information. Here, we fill this gap by developing a new gellan force field. Our simulations offer the first microscopic overview of gellan aggregation, detecting the coil to single-helix transition at dilute conditions and the formation of higher-order aggregates at high concentration through a two-step process: first, the formation of double helices and then their assembly into superstructures. For both steps, we also assess the role of monovalent and divalent cations, complementing simulations with rheology and atomic force microscopy experiments and highlighting the leading role of divalent cations. These results pave the way for future use of gellan-based systems in a variety of applications, from food science to art restoration.

## INTRODUCTION

Gellan is an anionic microbial exopolysaccharide that has gained increasing interest in the pharmaceutical, cosmetics, and food industry because of its functional and mechanical properties (1–5). It is a water-soluble, biocompatible, atoxic, biodegradable, and high-temperature chemically stable polymer (6, 7). Gellan is characterized by a linear structure consisting of tetrasaccharide repeating units, i.e., D-Glc($\beta 1 \rightarrow 4$)D-GlcA($\beta 1 \rightarrow 4$)D-Glc($\beta 1 \rightarrow 4$)L-Rha($\alpha 1 \rightarrow 3$) (8, 9). As a consequence, each repeating unit contains one carboxyl group belonging to the glucuronic acid that, when ionized in aqueous solution, confers the anionic character to the polysaccharide. The native polysaccharide also includes a L-glyceril and an acetyl group linked to the glucose moiety, which are industrially removed to produce a deacylated polymer, commonly known as gellan gum. The structure of polycrystalline fibers of the lithium salt of the deacylated gellan was determined by x-ray diffraction as consisting of a double helix formed by two left-handed, threefold helical chains (10), as lately confirmed also for the potassium form (11).

The most important property of gellan, which is at the origin of its widespread use, is the capability of forming thermoreversible transparent gels by cooling aqueous solutions containing cations, even at low polymer concentrations. The gellan sol-gel transition is an exothermic process (12) that can occur in a range of temperature between 30° and 50°C, depending on the specific nature of the cation, polymer concentration, and presence of cosolutes (13–16). In particular, it was observed that divalent cations determine a higher gelling temperature with respect to the monovalent counterpart (17). Cations were also found to affect the microstructure and the water holding capacity of gellan gels (18), as well as gel strength

(19). In addition, atomic force microscopy (AFM) measurements revealed that the network structure of gellan gels obtained with sodium chloride is more heterogeneous than that of gels formed in potassium chloride (20).

Another appealing property of gellan is its suitability as an innovative agent for wet cleaning treatments in the restoration of paper artworks (21). A recent work (22) also demonstrated that microgels based on gellan, i.e., microscale particles internally made by a gellan cross-linked network, offer several advantages for paper cleaning with respect to more established procedures based on wet cleaning or hydrogels systems. Paper is a complex material mainly formed by interwoven cellulose fibers, whose composition and structure can vary depending on the production process, which deteriorates with time due to environmental conditions (23–25). Because of the reduced size, microgels based on gellan can better penetrate the porous structure of paper and remove pollution and degradation materials in a shorter time (22). In addition, the softness of microgels suspensions can be adapted to the irregular surface of paper artworks, thus providing a higher efficiency. Note that gellan hydrogels used for paper cleaning are formed in the presence of calcium acetate (21), while gellan microgels are prepared by applying external shear upon the addition of sodium chloride (26). Clarifying the role of cations on gellan aggregation is, thus, important also in the context of cultural heritage applications of this polysaccharide.

The mechanism of gelation of gellan has been the source of many investigations. The main hypothesis is that of a two-step process (7, 27): In the first step, the gellan chains form double-helix structures, even in the absence of gel promoting cations (28); then, in a second step, the double helices form cation-mediated aggregates that compose the gel network. However, recent works based on statistical analysis of AFM images have also proposed that the first-ordered state is a single helix (29, 30), as also observed in the gelation mechanism of carrageenan, another anionic polysaccharide (31–33). Moreover, different interpretations of the two-step process still exist (27). On the basis of light scattering experiments, Gunning and Morris (34) proposed a model in which the first step consists in the formation of fibrils, composed of double helices formed

[1]CNR-ISC and Department of Physics, Sapienza University of Rome, Piazzale A. Moro 2, 00185 Rome, Italy. [2]Department of Chemical Science and Technologies, University of Rome Tor Vergata, Via della Ricerca Scientifica I, 00133 Rome, Italy. [3]Department of Chemical, Pharmaceutical and Agricultural Sciences, University of Ferrara, Via L. Borsari 46, 44121 Ferrara, Italy.
*Corresponding author. Email: letizia.tavagnacco@cnr.it (L.T.); emanuela.zaccarelli@cnr.it (E.Z.)

between ends of neighboring gellan chains, later followed by lateral crystallization of the fibrils mediated by cations, which ultimately leads to the formation of the gel. On the other hand, by using differential scanning calorimetry and rheology, Robinson *et al.* (*35*) proposed that gelation occurs first through a conversion from disordered coils (or single helices) into double-helix structures and then only some of these double helices form cation-mediated aggregates that compose the gel network. Hence, the second scenario includes a larger degree of disorder in the network, for the presence of disordered chains or unaggregated double helices, compatible with rheological signatures of weak gels.

Such a dispute has not been settled in the past 30 years, leaving unanswered (i) if and how single-helix and double-helix form and (ii) the role of cations in gel formation. To this aim, molecular dynamics simulations are a valuable tool since they allow for the investigation of these processes at the molecular scale. To perform this study, a force field for the gellan chains is needed, being not available in the literature. Only a recent study addressed the atomistic simulation of this polysaccharide but focusing on its acetylated form (*36*) that is not the one most widely used in applications because of its limited gelation ability (*7*).

Motivated by these reasons, in this work, we propose a new force field for (deacylated) gellan and perform extensive atomistic molecular dynamics simulations of chains under a variety of conditions, including the addition of monovalent and divalent salts. Comparing numerical results with AFM and rheology measurements, we characterize the microscopic process of gellan aggregation and unveil the role played by the cations. To validate our force field, we first confirm the occurrence of ion-induced single-helix structures under dilute conditions, in analogy with AFM studies (*29*, *30*). Next, we investigate the gelation mechanism at high concentrations, providing a microscopic explanation of the two-step gellan aggregation, which is the main focus of our study. First, we find that a conformational transition takes place from single- to double-helix structures, which can happen with and without the mediation of the cations. Second, we observe the association of double-helix structures into superaggregates through the complexation of carboxylate groups belonging to different double-helix structures. Our simulations further reveal a distinct behavior of the gellan chains in the presence of monovalent and divalent cations, because the latter are much more efficient in promoting the second step. Instead, for monovalent salt at the same charge content, we do not observe the formation of superaggregates in any of the simulated trajectories within the explored time window. Our results pave the way for a better microscopic understanding of the different structures observed in these largely used polysaccharide chains toward an improved control of the gelation mechanism, with direct impact on the wide variety of gellan applications.

## RESULTS
### Mechanical properties of gellan gels
The polysaccharide gellan is known to form physical gels through electrostatic interactions favored by the presence of cations. To characterize the molecular mechanism of formation of gellan gels and to understand the role played by the cations, first, we have carried out a qualitative investigation of the structure of gellan aggregates formed in different experimental conditions through AFM.

Figure 1 (A to C) directly compares the images of the polymer network obtained without adding salts to the polymer suspension ($G_{pure}$) and by adding sodium chloride ($G_{Na}$) or calcium acetate ($G_{Ca}$). We focus on results for $G_{Na}$ (27 mM) and $G_{Ca}$ (2.5 mM), because these are the salt concentrations relevant for application to paper preservation for microgels (*22*) and hydrogels (*21*), respectively.

While the networks of $G_{pure}$ and $G_{Na}$ (Fig. 1, A and B, respectively) show similar features, being composed by gellan aggregates of smaller size, aggregation in $G_{Ca}$ (Fig. 1C) appears more pronounced, as revealed by the distribution of the transversal size of polysaccharide filaments (aggregates), which widens and shifts at higher values (Fig. 1D). To determine the effect of the structural differences in the polymer network on the mechanical properties of the hydrogels, we performed rheological measurements on the same $G_{pure}$, $G_{Na}$, and $G_{Ca}$ samples. Figure 1E shows the storage and loss moduli $G'$ and $G''$ as a function of the shear strain $\gamma$. Under all conditions, the polymer network behaves as an elastic solid with $G'$ greater than $G''$. However, the addition of sodium causes a rise mostly of $G'$, while the addition of calcium induces an increase in both $G'$ and $G''$ revealing a different stability of the polymer network. We also tested aging effects by measuring the samples at different times after the preparation, and no substantial differences were detected (fig. S1). Figure 1E shows that the critical strain $\gamma_c$, which is defined as the intersection point between $G'$ and $G''$ and corresponds to the breaking point of the gel, occurs at slightly lower shear stress $\gamma$ when sodium is added to the polysaccharide suspension. Moreover $\gamma_c$ is strongly reduced in the presence of calcium, suggesting an increase in stiffness and a significantly different mechanical behavior of the gellan network formed with this divalent cation.

### Validation of the gellan force field in dilute conditions
To identify the molecular mechanism responsible for the differences in the macroscopic structural and mechanical features of gellan hydrogels, we exploited all-atom molecular dynamics simulations through our new gellan force field, as described in the "All-atom molecular dynamics simulations" section. First of all, we investigate the conformational behavior of a gellan chain in dilute conditions. Specifically, we consider a single chain in an aqueous solution of 0.05 M calcium acetate at a polymer concentration of $G_{Ca}$ [0.5 weight % (wt %)] and $T = 298$ K. Figure 2A shows the chemical structure of the gellan repeating unit. As described in Materials and Methods, we start the simulation from the x-ray diffraction structure of the gellan potassium salt (*11*), which is reported in Fig. 2B. To monitor the helix conformation in a qualitative way, we follow the evolution of the transversal component of the radius of gyration $R_t$. From the initial $R_t$ value of about 0.25 nm, the chain quickly adopts a helix conformation, which is characterized by a peaked distribution of $P(R_t)$, centered around 0.4 nm and with an SD of about 0.1 nm. These numbers are in qualitative agreement with those estimated from accurate AFM measurements on a solid surface (*29*, *30*), and the corresponding conformation, also illustrated in Fig. 2B, displays a helical shape. We then compare these results with those obtained for a single chain in the same aqueous environment but now interacting with the CHARMM36 (*37*) atomic partial charges. The corresponding results for $P(R_t)$, obtained starting from the same initial chain conformation, are also reported in Fig. 2B, showing a much less ordered structure,
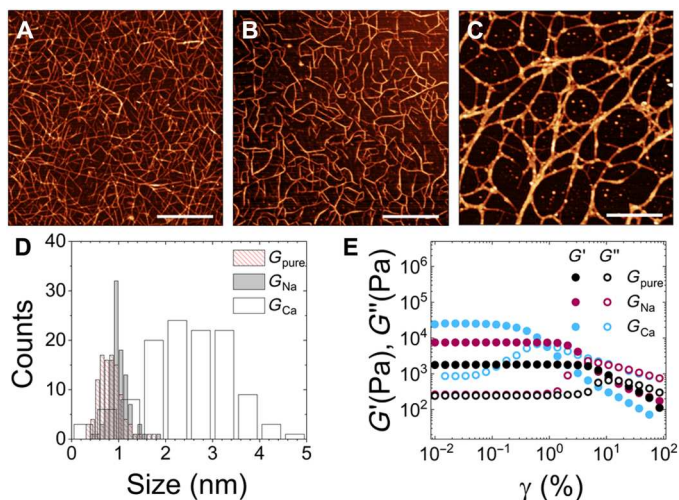
**Fig. 1. Macroscopic behavior of gellan gels.** AFM images of gellan hydrogels with a polysaccharide concentration of 2 wt % (**A**) without added salts, (**B**) with 27 mM sodium chloride, and (**C**) with 2.5 mM calcium acetate. Scale bars, 500 nm. (**D**) Histograms of size distribution of gellan chains determined by height profile. (**E**) Storage $G'$ (closed circles) and loss $G''$ (open circles) moduli as a function of shear strain $\gamma$ at $f = 1$ Hz and $T = 25°C$ for gellan hydrogels at a polysaccharide concentration of 2 wt % with 2.5 mM calcium acetate (light blue) or 27 mM sodium chloride (bordeaux) compared with pure gellan (black).



**Fig. 2. Gellan force field.** (**A**) Chemical structure of gellan repeating unit that is composed by four monosaccharides: D-glucose, D-glucuronic acid, D-glucose, and L-rhamnose that are shown in blue, red, blue, and gray, respectively. D-glucuronic acid is represented in the ionized form. Glycosidic linkages are shown in black. Atomic numbering is displayed on carbon atoms. (**B**) Distribution of the transversal component of the radius of gyration ($R_t$) calculated for the initial gellan conformation (blue dashed line) and from the simulation of a gellan chain in aqueous solution with 0.05 M calcium acetate at a polysaccharide concentration of 0.5 wt % with the gellan force field developed in this work (purple line) and with the CHARMM36 force field (orange line) at $T = 298$ K. The snapshots highlight the starting conformation (blue), a representative single-helix conformation sampled by the new force field (purple), and a typical disordered coil conformation detected in the CHARMM36 simulation (orange). In the snapshot of the starting conformation, the transversal component of the radius of gyration is also highlighted.

characterized by an asymmetric distribution also reaching much higher values up to 1 nm. This suggests that, under these conditions, mainly disordered coil conformations are sampled within the simulated trajectory. Because a strong evidence for single-helix conformation was reported in experiments, we conclude that the newly developed gellan force is superior to the CHARMM36 one in its ability to reproduce the correct chain conformations.

## Gelation mechanism at high concentrations

After these promising results for a single chain, we focus in the rest of the manuscript on the high-concentration regime to investigate gellan gelation mechanism. To this aim, we perform numerical simulations at ambient temperature (298 K) of a suspension of gellan chains in water at a polysaccharide mass fraction of 3, 5, and 10 wt %. In addition to the suspension of gellan chains in pure water, which contains only sodium ions as the carboxylate counterions (*38*), we investigate the behavior of gellan chains in aqueous solution of salt, particularly 0.1 M sodium chloride and 0.05 M calcium acetate. We study salt conditions bringing the same amount of positive charges to compare the effect of the chemical valence of the cation.

Figure 3 (A to I) displays some representative configurations of the gellan chains simulated at the different conditions. For the systems $G_{pure}$ and $G_{Na}$, aggregation of gellan chains is mainly detected only at the highest concentration of 10 wt %. Differently, for $G_{Ca}$, association of gellan chains is observed even at the lowest concentration of 3 wt %, and it becomes more extended at higher polysaccharide concentrations. We note that, independently on the investigated aqueous solution conditions, in all our simulations, association of pairs of gellan chains occurs through the formation of double-helix structures, as illustrated in Fig. 4A, in agreement with previous experiments at similar concentrations (*28*, *39*). Because of
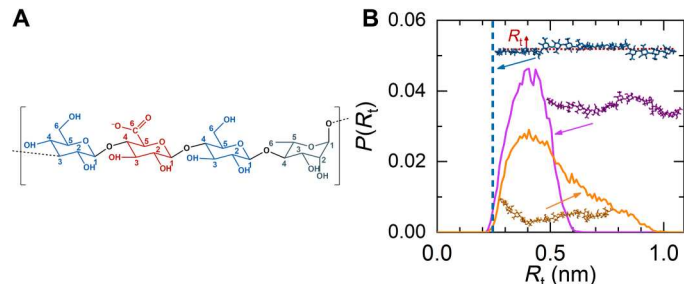
the limited size of the simulation model, which may hinder the aggregation of the chains under the studied dense conditions, we also tested the reproducibility of the results by performing additional 10 independent replicas of the systems $G_{Na}$ (5 wt %) and $G_{Ca}$ (5 wt %). We found double-helix association of gellan chains with a probability of 45% for the former and with a probability of 73% for the latter (see figs. S2 and S3). These results allow us to consider the solution behavior of the replicas reported in Fig. 3 (E and F) as representative examples of the explored conditions. In addition, we have further inspected our proposed gellan force field, by comparing simulations results for the system $G_{Ca}$ (5 wt %), in which strong aggregation is observed, with those obtained in additional simulations carried out using CHARMM36 (*37*) atomic partial charges under the same conditions (see table S1). Again, we performed 10 independent replicas, without finding in any case the formation of double-helix structures, as illustrated in fig. S4.

We now characterize in more detail the aggregation of gellan chains in aqueous solution by evaluating the radial distribution functions of the gellan oxygen atoms belonging to the carboxylate group of the D-glucuronic acid (see the chemical structure of the repeating unit shown in Fig. 2A). The results are summarized in Fig. 4 (B to J), which displays all the distribution functions calculated for each individual chain with respect to the others. For the systems $G_{pure}$ and $G_{Na}$, the radial distribution functions show well-defined peaks at ~8 and ~12 Å only at the concentration of 10 wt %. Instead, in the case of $G_{Ca}$ at all concentrations, two peaks are detected at the same distances. By analyzing the structure of the double helix formed by the association between two gellan chains (Fig. 4A), it is possible to assign the two peaks to pairs of oxygen atoms, each of them belonging to a different chain. Due to the conformation of the double helix, the pairs can be pointing either toward the same (~8-Å) or toward the opposite (~12-Å) direction, as shown in Fig. 4A. The lowest height peaks that arise at shorter distances mainly in $G_{Ca}$ can be attributed to less frequent
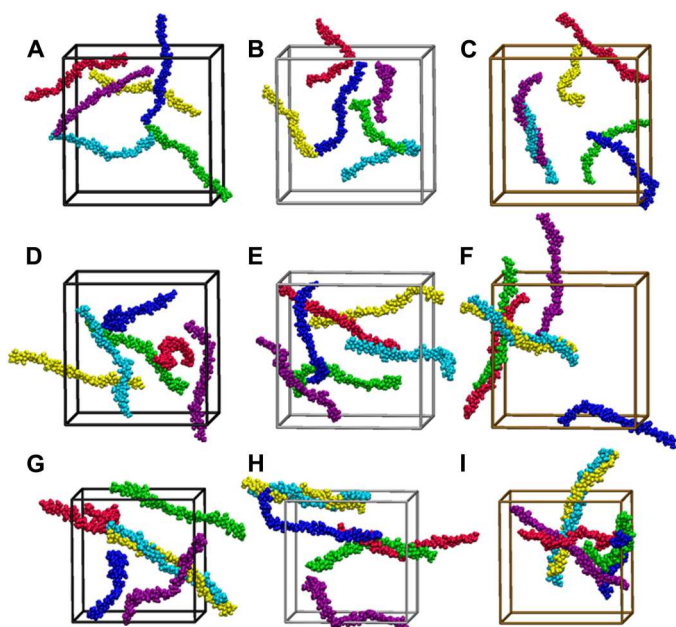
**Fig. 3. Molecular dynamics simulations results.** Representative snapshots from all-atom simulations at 298 K of pure gellan (black simulation box) at concentration of (**A**) 3 wt %, (**D**) 5 wt %, and (**G**) 10 wt %; gellan with 0.1 M sodium chloride (gray simulation box) at a polysaccharide concentration of (**B**) 3 wt %, (**E**) 5 wt %, and (**H**) 10 wt %; and gellan with 0.05 M calcium acetate (gold simulation box) at a polysaccharide concentration of (**C**) 3 wt %, (**F**) 5 wt %, and (**I**) 10 wt %. Each polysaccharide chain is shown with a different color. Ions and water molecules are omitted for clarity.

contacts between gellan chains not associated in a double-helix structure. In particular, in the presence of calcium ions at the highest gellan concentration, a transient aggregation of chains 3 and 4 has been detected (Fig. 4J).

We further investigate the solution structuring by monitoring the hydrogen bonding interactions formed by the gellan chains and those occurring between water and the polysaccharide, as reported in Fig. 5 (A and B). The average number of intra- and inter-chain hydrogen bonds formed by gellan is higher in the presence of calcium, and, differently from $G_{pure}$ and $G_{Na}$, in which it increases with the polysaccharide content, a nonmonotonic concentration dependence is observed in $G_{Ca}$ (Fig. 5A), in agreement with the experimental observation that high salt concentrations cause a decrease in gel strength (*7*). The number of hydrogen bonds between associated gellan chains appears to be stable, as shown by the time evolution of the gellan hydrogen bonds formed by each chain with all others which is reported in fig. S5. In addition, the calcium cation not only favors the interactions between gellan chains but also increases the structuring of hydration water molecules, promoting a higher average number of water-gellan hydrogen bonds in the whole concentration range explored (Fig. 5B).

We now examine the conformation of the polysaccharide in aqueous solution. Figure 6 (A to I) reports the distribution of radius of gyration of each individual chain for the different conditions explored. In the systems where no aggregation is detected, such as $G_{pure}$ (3 wt %) (Fig. 6A) or $G_{Na}$ (3 wt %) (Fig. 6B), gellan chains assume a similar broad distribution of radius of gyration. Conversely, when association occurs, the conformation of gellan

chains involved in the formation of aggregates can be distinguished from the others. For example, in the system $G_{Ca}$ (5 wt %) (Fig. 6F), the polysaccharide chains that are associated to other chains, as determined in Figs. 3F and 4G, have a narrow distribution of radius of gyration with a maximum at ~2.2 nm. Moreover, chains that form a partial double-helix structure (red and green chains in Fig. 6F) are characterized by a broader distribution of radius of gyration with respect to those fully paired (cyan and yellow chains in Fig. 6F). The crowding effect of the polymer chains can also induce the population of conformational states with lower values of the radius of gyration (red chain in Fig. 6I). These findings suggest that gellan aggregation occurs through a conformational transition of the polysaccharide chains, which leads to rigid elongated conformations. The lower flexibility of associated gellan chains is also detectable by monitoring the time evolution of the radius of gyration of each polysaccharide chain, as displayed in fig. S6. For example, in the system $G_{Ca}$ (5 wt %) (fig. S6F), the fluctuations of the values of the radius of gyration for associated chains (cyan and yellow chains) are considerably reduced as compared to the other chains (purple and blue chains). To understand in more detail the molecular origin of the flexibility of gellan chains, we have further analyzed the behavior of the dihedral angles of the glycosidic linkages between the monosaccharides composing the chains. Because of the hindered torsion of sugar ring bonds, the rotation around the glycosidic linkage is the mechanism that confers to the polysaccharide partial flexibility. We have thus evaluated the number of transitions of all the glycosidic dihedral angles of each gellan chain Φ, defined as H1-C1-O1-C4′, and Ψ, defined as C1-O1-C4′-H4′, as illustrated in the scheme of fig. S7 and shown in figs. S8 (A to I) and S9 (A to I). The results indicate that the rotation of the dihedral angle Φ is quite restricted, independently on the gellan concentration, added salt, or aggregation state of the chain. In the case of the dihedral angle Ψ, we observe that (i) transitions are mostly detected for glycosidic linkages to glucose residues; (ii) no direct correlation with the nature of the cation added is observed; and (iii) the dihedrals transitions are hindered for associated gellan chains, determining the increased stiffness of aggregated systems.

Because of the present simulation results, we now tackle the two main open questions about gellan aggregation mechanism. First, we address the issue of helix formation. The results reported so far illustrate that double helices form in the presence of calcium at all studied gellan concentrations. The dominant role of electrostatic interactions is also shown by comparing their contribution to the total energy, as reported in table S2. However, while it appears that divalent cations facilitate the occurrence of double helices, they can also form just in the presence of added sodium or in pure gellan. In this respect, it is useful to recall that, even in pure gellan, there is an amount of dissolved electrolyte. For example in our simulations, each polysaccharide chain adds to the solution 4 sodium counterions for a total of 24 ions in every simulated system. As a comparison, the gellan suspension at concentration of 5 wt % in 0.1 M sodium chloride contains 58 sodium ions, 24 of them being the gellan counterions. Hence, at high enough gellan concentration, gellan counterions themselves will have an effect on the aggregation process. We now want to discriminate the specific role of the cations by assessing what is their contribution to the double-helix formation with a closer look to how cations are arranged with respect to a chain. We start by focusing on the carboxylate groups because we expect these to be the ones undergoing more significant
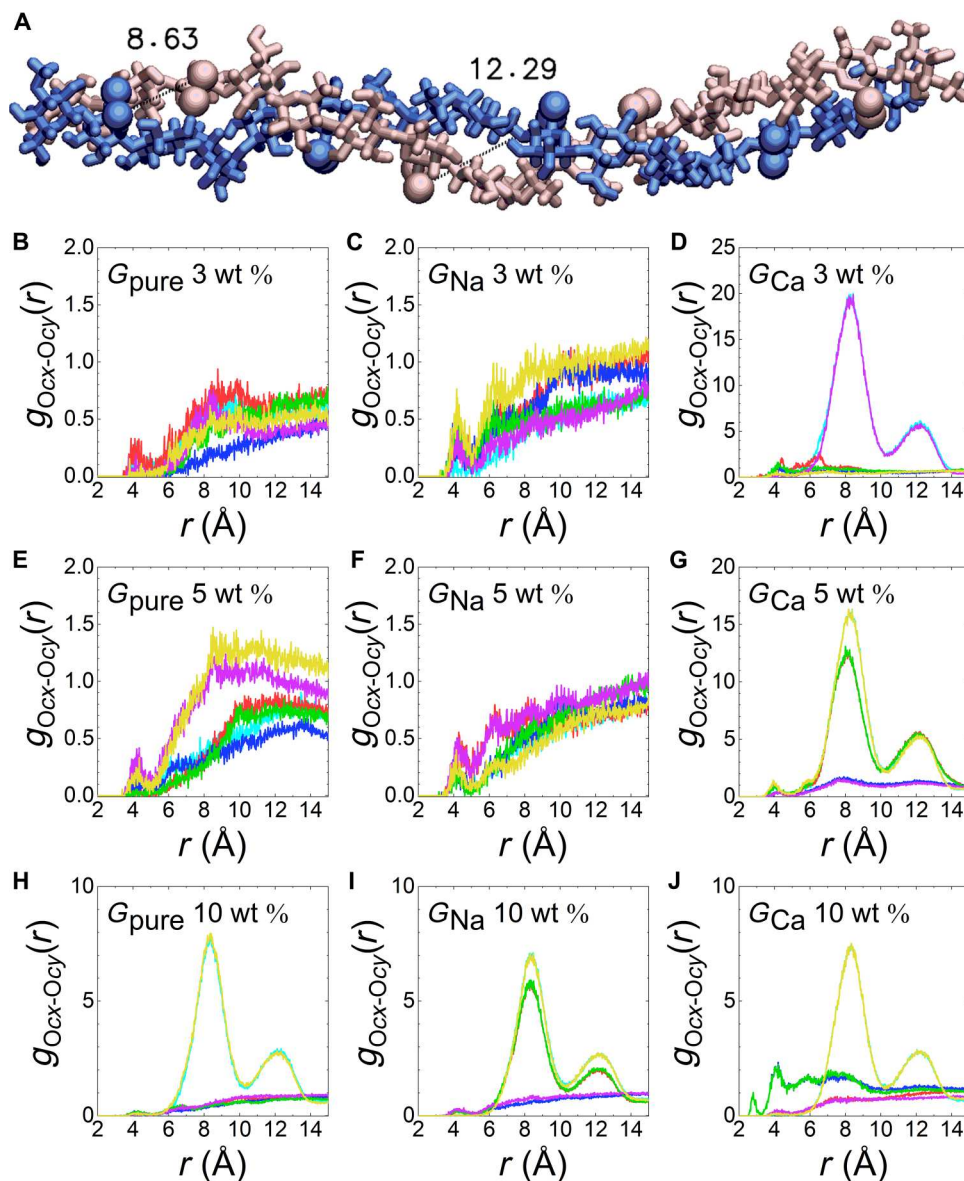
**Fig. 4. Double-helix conformation.** (**A**) Double-helix structure formed from the association of two gellan chains in the system $G_{Ca}$ (5 wt %). Oxygen atoms belonging to the carboxylate group of the D-glucuronic acid unit and their characteristic interchain distances (in angstroms) are highlighted in the representation. Radial distribution functions for gellan oxygen atoms of the carboxylate group of the chain ($C_x$) with respect to all other chains ($C_y$) calculated at 298 K for pure gellan at concentration of (**B**) 3 wt %, (**E**) 5 wt %, and (**H**) 10 wt %; gellan with 0.1 M sodium chloride at a polysaccharide concentration of (**C**) 3 wt %, (**F**) 5 wt %, and (**I**)10 wt %; and gellan with 0.05 M calcium acetate at a polysaccharide concentration of (**D**) 3 wt %, (**G**) 5 wt %, and (**J**) 10 wt %. Data calculated for chains 1, 2, 3, 4, 5, and 6 are shown in cyan, red, blue, green, purple, and yellow, respectively. Radial distribution functions are averaged over the last 100-ns trajectory.

interactions with the cations due to their opposite charge and report the radial distribution functions for sodium or calcium with respect to the gellan oxygen atoms of these groups $g_{O-Na/Ca}(r)$ in Fig. 7 (A to L) for all studied state points. In particular, every plot reports six curves corresponding to each gellan chain in the simulations, so that we can discriminate the behavior of those chains involved in double-helix formation. For all cases, we observe the presence of two peaks in $g_{O-Na/Ca}(r)$ at short distances, roughly located at the same two distances for all chains, independently of their aggregation state. In particular, a first peak occurs around 2.3 Å, corresponding to cations directly interacting with the carboxylate oxygens

(snapshots in Fig. 7M), followed by a second peak located around 4.5 Å. The latter distance is compatible either with cations being on opposite side of the chains with respect to the considered oxygen atoms or with those "bridging" two chains forming a helix (snapshots in Fig. 7N). We note that the intensity of both peaks is approximately 10 times larger in the case of calcium with respect to sodium. Focusing on chains exhibiting double-helix formation, we find an enhancement of the second peak in the presence of sodium ions (Figs. 7, I and J), while a huge variation is detected for calcium (Fig. 7, D, H, and L) that is also accompanied by a significant growth of the first peak. These results prove, at the
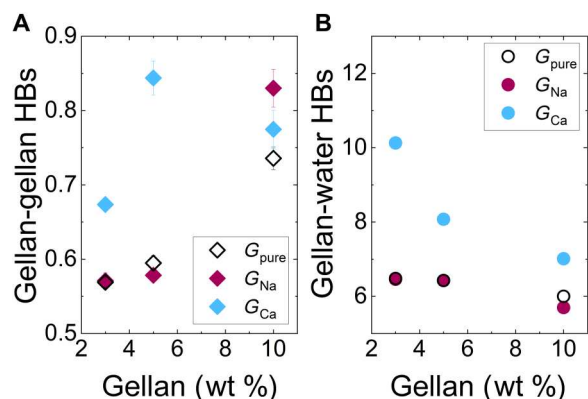
**Fig. 5. Hydrogen bonding interactions.** Average number of gellan-gellan (**A**) and gellan-water (**B**) hydrogen bonds (HBs) normalized to the number of monosaccharides and averaged over the last 100 ns of simulations as a function of the gellan concentration. Data calculated for the simulations of gellan without added salts, with sodium chloride, and with calcium acetate are shown in black, bordeaux, and light blue, respectively. Errors are estimated by the blocking method.
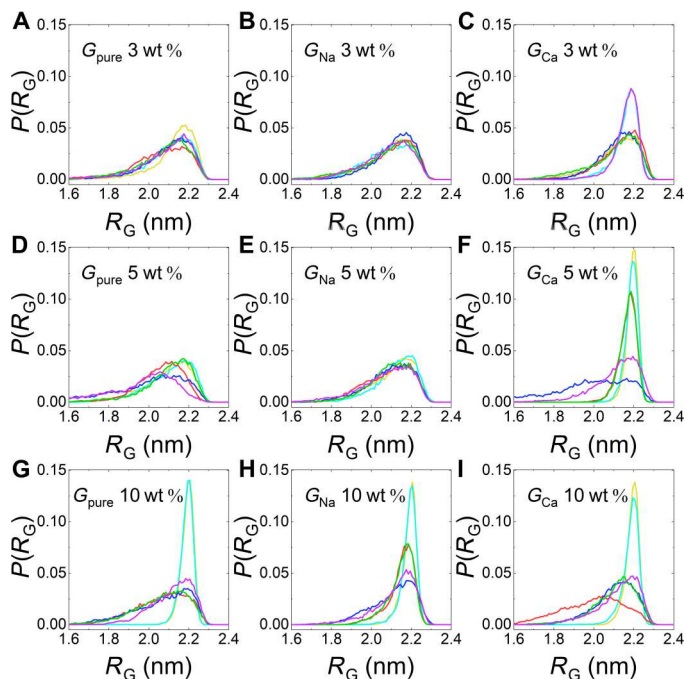


**Fig. 6. First aggregation step.** Distribution of the radius of gyration [$P(R_G)$] of each gellan chain at 298 K calculated for pure gellan at concentration of (**A**) 3 wt %, (**D**) 5 wt %, and (**G**) 10 wt %; gellan with 0.1 M sodium chloride at a polysaccharide concentration of (**B**) 3 wt %, (**E**) 5 wt %, and (**H**) 10 wt %; and gellan with 0.05 M calcium acetate at a polysaccharide concentration of (**C**) 3 wt %, (**F**) 5 wt %, and (**I**) 10 wt %. Data calculated for chains 1, 2, 3, 4, 5, and 6 are shown in cyan, red, blue, green, purple, and yellow, respectively.

microscopic level, that both sodium and calcium ions are involved in the formation of the double helix. Because the behavior of $g_{O-Na}(r)$ at high polysaccharide concentration (10 wt %) is almost identical for pure gellan and for gellan with added NaCl (Fig. 7, I and J, respectively), we deduce that double-helix formation takes

place even in the absence of added salt but always through the mediation of the cations. This is signaled by the increase in the second peak of the radial distribution functions for helix-forming chains, which is compatible with the appearance of configurations where the cations are in between the two chains (see snapshots in Fig. 7N). Instead, the huge change observed in the calcium arrangement around helix-forming chains highlights the dominant role of divalent ions, which trigger the helix formation at all studied gellan concentrations. Given that, for sodium, the same is true only at large gellan concentrations [or presumably at high sodium concentrations, as suggested by experiments (*35*)], the present results show that monovalent salt ions only mediate helix formation as a consequence of their high density.

Having shed light on the double-helix formation, we now turn to the second step of gellan aggregation. Notwithstanding that the data collected in atomistic simulations are limited in size, time, and number of examined state points, our findings provide a robust evidence of the crucial role of divalent ions in this second step. Only for calcium acetate we have observed, within our numerical accuracy, the onset of the bonding of two double helices, coherently with the increased aggregate size measured by AFM (Fig. 1D). Because this occurs only for the specific gellan concentration of 5 wt %, we now focus on this case. To accurately probe the solution behavior, we averaged the simulation results over all independent simulations performed for these conditions (a total of 11 simulations for each salt). Figure 8 shows the radial distribution function of the different cations with respect to the polysaccharide chains. Differently from the data shown in Fig. 7, here, we do not discriminate among different chains and average results over all chains. We thus compare the findings for $g_{O\ all\text{-}cation}(r)$, sampled for sodium or calcium cations close to all gellan oxygen atoms in Fig. 8A with the radial distributions calculated between gellan oxygen atoms of hydroxyl groups (Fig. 8B) or carboxylate groups (Fig. 8C) and the cations. Comparing the three panels for sodium ions, we find that their average arrangement is independent of the presence of calcium. In particular, the first peak is much more pronounced near hydroxyl groups, while the second peak is larger near carboxyl groups. However, the results for calcium ions show a much more ordered arrangement: With respect to sodium, we find ≈3-fold increase at the first and second peaks of the hydroxyl groups, which becomes ≈50- and 10-fold for the carboxylate groups, respectively. Concerning the interaction distances, we find that the position of the first peak is roughly the same for both ions close to all gellan groups. Instead, the second peak for sodium is slightly larger for hydroxyl groups than that for carboxyl ones, and, in the latter case, its position coincides with the one observed for calcium ions.

Because the positions of the two first peaks are the same as those discussed in Fig. 7 (A to L), the characteristic cation arrangement must belong to the cases described before. To reveal the presence of superaggregates, we cannot rely on the distance; therefore, we count how many chains are close to each cation within our simulation trajectories. The resulting distributions $n_{cation}$, denoting the number of cations having $n_C$ neighboring chains, are reported in Fig. 8 (D and E, respectively), for the two characteristic regions: 0 to 4 Å for those in direct contact and 4 to 6 Å for those mediating double helices and superaggregates. We observe that for the first shell, very few cations exceed one neighboring chain, with calcium ions being preferentially closer to them. However, in the second shell, a few sodium ions close to two chains appear, as
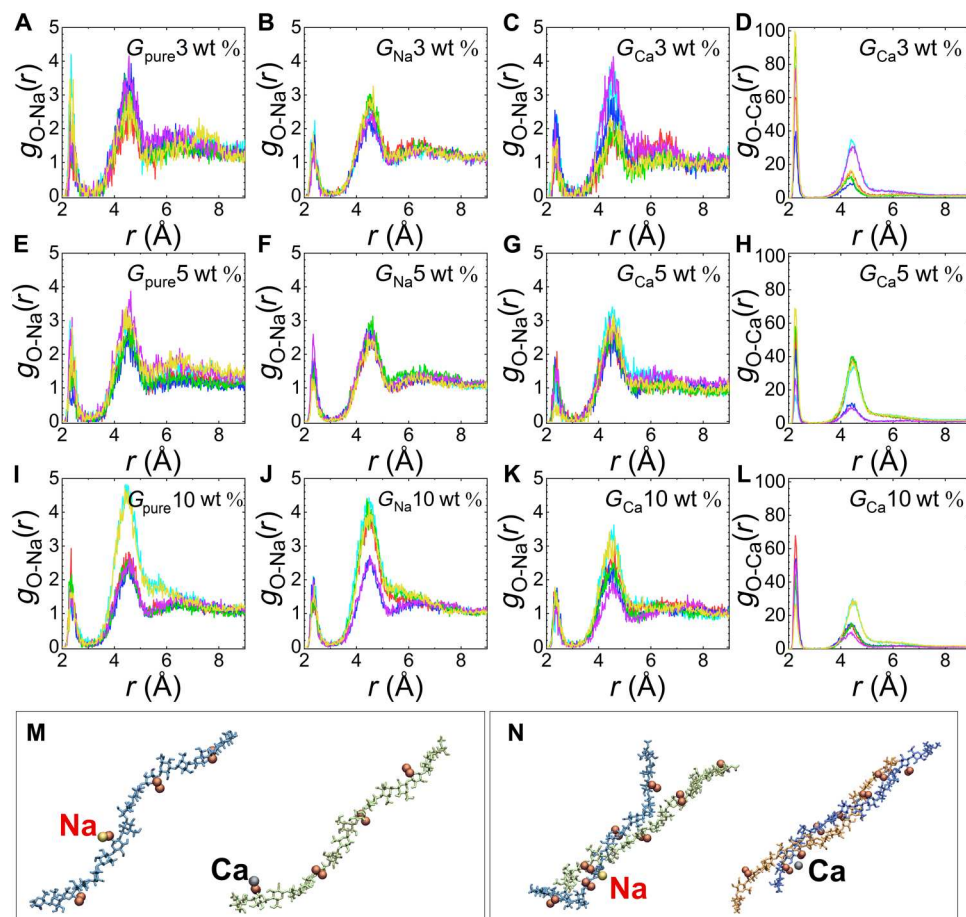
**Fig. 7. Role of monovalent and divalent cations.** Radial distribution functions for sodium cations around the gellan oxygen atoms of the carboxylate group of each chain calculated at 298 K for pure gellan at concentration of (**A**) 3 wt %, (**E**) 5 wt %, and (**I**) 10 wt %; gellan with 0.1 M sodium chloride at a polysaccharide concentration of (**B**) 3 wt %, (**F**) 5 wt %, and (**J**) 10 wt %; and gellan with 0.05 M calcium acetate at a polysaccharide concentration of (**C**) 3 wt %, (**G**) 5 wt %, and (**K**) 10 wt %. Radial distribution functions for calcium cations around the gellan oxygen atoms of the carboxylate group of each chain calculated at 298 K for gellan with 0.05 M calcium acetate at a polysaccharide concentration of (**D**) 3 wt %, (**H**) 5 wt %, and (**L**) 10 wt %. Data calculated for chains 1, 2, 3, 4, 5, and 6 are shown in cyan, red, blue, green, purple, and yellow, respectively. Radial distribution functions are averaged over the last 100-ns trajectory. Representative snapshots showing the arrangement of calcium and sodium around gellan carboxylate groups of (**M**) a single chain or (**N**) a double helix. Sodium and calcium are shown in yellow and gray, respectively. Oxygen atoms of the gellan carboxylate groups are displayed in ochre.

well as very rare events of three-chain connection, with a similar behavior in both $G_{Na}$ (5 wt %) and $G_{Ca}$ (5 wt %). The most significant result is found for calcium ions: Despite the fact that they are the lowest in number (only 17 in each run), they show the largest number not only close to two chains but also close to three and four chains, for the presence of the junction between two double helices. The latter finding provides unambiguous evidence that calcium ions promote superaggregate formation, even in our very reduced and idealized simulation environment, as shown in the snapshot reported in Fig. 8F.

## DISCUSSION
In this work, we developed an atomistic model for the polysaccharide gellan to probe its gelation mechanism at the molecular scale. By performing extensive molecular dynamics simulations as a function of the polysaccharide concentration and with the addition of monovalent or divalent salts, we first detected the conformational transition from a coil to a single helix in dilute regime and then explored in detail the gellan gelation process at high concentrations and the specific role played by cations. Within the size and time limitations of atomistic simulations, our findings provide evidence that gellan aggregation is a two-step process strongly affected by the nature of the cations involved. At the examined gellan concentrations, the first step involves the formation of a double helix. Then, aggregation of double helices into superstructures occurs in the second step. Our analysis suggests that a single helix is more rarely seen at high concentrations, probably due to the interactions with all other chains, so that the primary structure for gel formation is that of a double helix. However, several recent works have demonstrated that, at intermediate polysaccharide concentrations, such as between the extremely diluted concentrations needed for the emergence of single helices and the high concentrations required for rheological gelation, the structural evolution from single helix to extended aggregates occurs through a coil-coil aggregation rather than by assembling into double helices (*29–33*). Thus, it
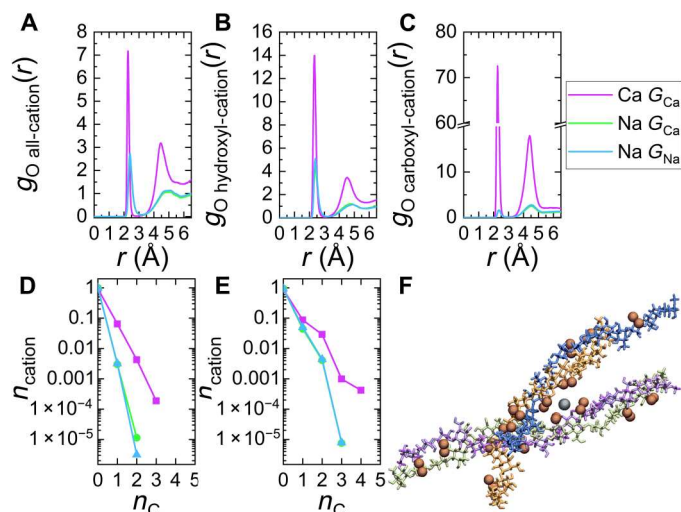
**Fig. 8. Second aggregation step.** Radial distribution functions for cations around (**A**) all gellan oxygen atoms, (**B**) gellan oxygen atoms of the hydroxyl groups, and (**C**) gellan oxygen atoms of the carboxylate group calculated over the last 100-ns trajectory and averaged over 11 independent simulations. Distribution of the number of cations ($n_{cation}$) having $n_c$ neighboring chains within a distance $d$, such that $0\ \text{Å} \le d \le 4\ \text{Å}$ (**D**) and $4\ \text{Å} \le d \le 6\ \text{Å}$ (**E**), calculated over the last 100-ns trajectory, averaged over 11 independent simulations, and normalized to the total number of cations. Data refer to the systems with gellan concentration of 5 wt % with 0.1 M sodium chloride (blue) and with 0.05 M calcium acetate for sodium (green) and calcium (purple). (**F**) Representative snapshot showing a superaggregate between two double-helix structures bridged by calcium, which is shown in gray. Oxygen atoms of the gellan carboxylate groups are displayed in ochre.

will be interesting in the future to perform a systematic study bridging the low- and high-concentration regime to possibly detect a different state at intermediate gellan densities. In addition, it may be worthy to investigate the effect of a nearby surface on the chain conformation, which could play a role in this aspect as suggested by AFM measurements (*29*, *30*).

The present results also allow us to shed light on the different roles played by monovalent and divalent cations. They suggest that divalent salt promotes in a rapid (because it happens within the duration of our simulations) and efficient (because it happens in the large majority of trajectories) aggregation of gellan chains. This is in agreement with the proposed interpretation of Gunning and Morris (*34*), where a highly coherent superstructure and degree of cross-linking should be formed, as a sort of "strong gels." A recent AFM investigation has also reported the formation of thick gellan fibrillar structures by lateral aggregation in the presence of calcium, confirming the extended aggregation promoted by divalent cations (*30*). However, sodium ions, both as gellan counterions and as added electrolyte, surely participate to the mechanism and contribute to the formation of double helices, also detected in our simulations, but their role in the formation in the superaggregates is more limited. This is in agreement with the fact that monovalent cations become more efficient at high enough gellan concentration, as experimentally detected (*17*) and also shown in Fig. 4 (H and I). It is thus probable that gels obtained in the presence of monovalent salt are more disordered, with an overall lower degree of cross-linking and likely the presence of chains not assembled into double helices,

giving rise to weaker gels, in agreement with the hypothesis of Robinson *et al.* (*35*).

Our investigation can be extended in the near future to study the aggregation mechanism of acylated and low-acylated gellan, in which the presence of acyl substituents increases the complexity of the aggregation process by conferring to the polysaccharide hydrophobic properties that can also lead to hydrophobic association and could inhibit or even preempt the formation of double helices. In this perspective, the use of atomistic simulations could be again crucial to discern between molecular mechanisms of aggregation that can generate different structure-property functions of the material, thus allowing to identify the optimal conditions with respect to the specific application requirements.

## MATERIALS AND METHODS
### Sample preparation
Deacylated gellan (KELCOGEL CG-LA), also known as gellan gum and, hereafter, referred to as gellan, was purchased from CP Kelco (Atlanta, GA, USA). Calcium acetate and sodium chloride are from Merck (Merck KGaA, Darmstadt, Germany). Ultrapure water (Milli-Q, Millipore, Billerica, MA, USA) was used in the preparation of solutions (resistivity of 18.2 megaohm·cm at $T = 25°C$). Three different systems were compared: gellan hydrogels without added salts ($G_{pure}$), hydrogels with sodium chloride ($G_{Na}$), and hydrogels with calcium acetate ($G_{Ca}$). To prepare pure hydrogels ($G_{pure}$), gellan powder was dispersed in ultrapure water at room temperature. The dispersion, previously purified by dialysis using dialysis tubing with 12,400-Da cutoff, was first heated up in the microwave oven until it became transparent and, then, for rheological measurements, it was poured into petri dishes at room temperature to obtain a gel thickness of about 4 to 5 mm. $G_{pure}$ was investigated at a polysaccharide mass fraction of 2 wt %. Hydrogels containing calcium or sodium ions were obtained by dissolving gellan and a proper amount of corresponding salt in water and by following the same protocol described for the hydrogels without added salts. Hydrogels with added salts were also prepared at a polysaccharide mass fraction of 2 wt %. $G_{Na}$ was prepared at a sodium chloride concentration of 27 mM, while $G_{Ca}$ was obtained at a calcium acetate concentration of 2.5 mM.

### Rheological measurements
Rheological measurements were performed with a Rheometer MCR102, Anton Paar, with a plate-plate geometry (diameter, 49.97 mm) equipped with a Peltier system to control temperature, an evaporation blocker, and an isolation hood to prevent solvent evaporation. Measurements were performed through a ReoCompass software. Storage ($G'$) and loss ($G''$) moduli were measured at $T = 25°C$ as a function of shear strain $\gamma$ at frequency $f = 1$ Hz, in linear viscoelastic regime. Measurements were carried out ~18 and ~43 hours after preparation to test aging effects and reproducibility.

### AFM measurements
AFM measurements were performed with a Dimension Icon (Bruker AXS) instrument. Images were acquired in air, at room temperature, and under ambient conditions in Tapping mode to protect the samples from damage. To maximize the image resolution, a rotated tapping etched silicon probe (Bruker, Germany) with

a nominal radius of curvature $R \leq 8$ nm was used. For all the AFM measurements, samples have been deposited on freshly cleaved mica, incubated less than 1 min, then rinsed with Milli-Q water, and analyzed. Images have been corrected by leveling and background subtraction using Gwiddion 2.56 free software. A minimum of 100 height profiles of aggregates have been used for size histograms.

## All-atom molecular dynamics simulations
### Gellan force field
Starting atomic coordinates for the repeating unit of gellan were taken from the reported x-ray diffraction structure of oriented fibers of the gellan potassium salt (11). In this structure, the conformation of glycosidic linkages falls in minimum energy domains (40). Gellan force field was developed using the parameters values for the bonds, angles, dihedrals, and improper dihedrals based on the CHARMM36 force field (37) for carbohydrates and by computing atomic partial charges. Charge calculation was performed on the gellan repeating unit having a methyl group bonded to the oxygen atoms of carbon 3 of D-glucose and carbon 1 of L-rhamnose (Fig. 2A) to mimic the chain extension. To estimate electronic densities, quantum mechanical calculations were carried out using the Gaussian16 software (41). The geometry of gellan was optimized at the B3LYP/6-31g(d) level of theory. In the calculation, a dielectric continuum was used to simulate the solvent effect, as previously reported (40). Single-point energy calculation on the geometry optimized gellan configuration was carried out at the HF/6-31g(d) level of theory. Effective charges were calculated using the restrained electrostatic potential (RESP) method (42).

## Simulation protocol
All-atom molecular dynamics simulations were performed on a dispersion of gellan chains in aqueous solution to characterize the mechanism of aggregation. A gellan chain consists of four repeating units, overall corresponding to 16 monosaccharides, and it is endcapped by methoxy groups. The degree of polymerization (DP) of gellan chains has been optimized to sample a significant number of interchain processes in the time scale accessible to the simulations. The lower DP of polymer chains in simulations as compared to experiments could originate a variation under gelation conditions but preserving the validity of the comparison between simulated models. In all simulations, gellan was described using the newly developed force field, except for a representative case study of the system $G_{Ca}$ (5 wt %), that was also carried out directly using CHARMM36 (37) atomic partial charges, as in (36). This was done to validate the force field developed in this work. A further assessment of the force field was carried out by performing a simulation of a single-gellan chain at 298 K and at a concentration of $G_{Ca}$ (0.5 wt %) to mimic the diluteconditions at which coil to single-helix transition was observed through AFM measurements (29, 30). This was performed again for our newly developed force field and using CHARMM36 directly. In all cases, salts and water were described using the CHARMM36 (37) and TIP3P (43) force fields, respectively. To investigate the effects of polysaccharide concentration and added salts, several experimental conditions were explored. In particular, simulations were carried out at gellan mass fraction of 3, 5, and 10% without salts and by adding sodium chloride or calcium acetate. Simulations with sodium chloride were performed with a salt concentration of 0.1 M. Simulations with calcium acetate

were carried out with a salt concentration of 0.05 M, thus maintaining the same number of charges brought in solutions by the cations. The electrostatic stoichiometry was used as a comparison parameter because, in the atomistic description, it allows for a clearer interpretation, rather than ionic strength that should be preferred in models accessing much larger space domains. We assumed that the difference in anions of our models negligibly influences the results, because the effect of chloride and acetate ions on gellan association is comparable, both anions favoring the gelation irrespective of concentration of added electrolyte (44). Because of the limits imposed by the atomistic description to the overall size of the models, the concentrations of polymer and added salts in the simulations are higher than those used in experiments. The selected composition of the gellan solution models allowed for the insertion of a representative number of molecular species, with a sustainable computing cost. To test the reproducibility of the simulations results, independent replicas were carried out for the systems $G_{Na}$ (5 wt %) and $G_{Ca}$ (5 wt %), the latter also for the CHARMM36 force field.

For each simulation at high concentrations, six energy-optimized gellan chains with deprotonated glucuronic acid units were first inserted in a cubic box and oriented to maximize the distance between each other. Then, the number of TIP3P water molecules and sodium counterions corresponding to the set concentration were added and another energy minimization with tolerance of 100 kJ mol$^{-1}$nm$^{-1}$ was carried out. The resulting system was equilibrated at 298 K for 40 ns and heated upto 353 K at 1 K ns$^{-1}$. After these steps, for the simulations with added salts, a number of ions corresponding to the set concentration was added to the configuration at 353 K, and the system was equilibrated for 40 ns at 353 K. Simulations were then carried out for 160 ns at 353 K. Last, the system was cooled to 298 K at 1 K ns$^{-1}$ and equilibrated at 298 K for 40 ns, and trajectory data were acquired for 160 ns at 298 K. This simulation protocol, and particularly the insertion of added salt into the gellan solution at 353 K, was chosen to mimic the preparation of gellan microgels put forward in (22, 26). All simulations were carried out in the isothermal-isobaric (NPT) ensemble. The leapfrog integration algorithm (45) with a time step of 2 fs was used. Cubic periodic boundary conditions and minimum image convention were applied. The length of bonds involving H atoms was constrained by the linear constraint solver (LINCS) procedure (46). The velocity rescaling thermostat coupling algorithm, with a time constant of 0.1 ps, was used to control temperature (47). During equilibration, pressure was maintained by using the Berendsen barostat (48) with a time constant of 1 ps. During data acquisition, a pressure of 1 atm was maintained by the Parrinello-Rahman barostat, with a time constant of 2 ps (49, 50). The cutoff of nonbonded interactions was set to 1 nm. Electrostatic interactions were calculated by the smooth particle-mesh Ewald method (51). Trajectories were acquired with the GROMACS software package (version 2018) (52, 53), and the last 100 ns were considered for analysis, sampling one frame every 5 ps.

## Supplementary Materials
This PDF file includes:
Figs. S1 to S9
Tables S1 and S2

## REFERENCES AND NOTES

1. T. Osmałek, A. Froelich, S. Tasarek, Application of gellan gum in pharmacy and medicine. *Int. J. Pharm.* **466**, 328–340 (2014).

2. M. Matsusaki, H. Ikeguchi, C. Kubo, H. Sato, Y. Kuramochi, D. Takagi, Fabrication of per-fusable pseudo blood vessels by controlling sol–gel transition of gellan gum templates. *ACS Biomater Sci. Eng.* **5**, 5637–5643 (2019).

3. M. Müller, P. Fisch, M. Molnar, S. Eggert, M. Binelli, K. Maniura-Weber, M. Zenobi-Wong, Development and thorough characterization of the processing steps of an ink for 3D printing for bone tissue engineering. *Mater. Sci. Eng. C* **108**, 110510 (2020).

4. S. Liu, Y. Qiu, W. Yu, H. Zhang, Highly stretchable and self-healing strain sensor based on gellan gum hybrid hydrogel for human motion monitoring. *ACS Appl. Polym. Mater.* **2**, 1325–1334 (2020).

5. C. Villarreal-Otalvaro, J. M. Coburn, Fabrication methods and form factors of gellan gum–based materials for drug delivery and anti-cancer applications. *ACS Biomater. Sci. Eng.*, 10.1021/acsbiomaterials.1c00685 (2021).

6. R. Chandrasekaran, A. Radha, Molecular architectures and functional properties of gellan gum and related polysaccharides. *Trends Food Sci. Technol.* **6**, 143–148 (1995).

7. C. Iurciuc, A. Savin, C. Lungu, P. Martin, M. Popa, Gellan. Food applications. *Cellulose Chem. Technol.* **50**, 1–13 (2016).

8. P.-E. Jansson, B. Lindberg, P. A. Sandford, Structural studies of gellan gum, an extracellular polysaccharide elaborated by *Pseudomonas elodea. Carbohydr. Res.* **124**, 135–139 (1983).

9. M. A. O'Neill, R. R. Selvendran, V. J. Morris, Structure of the acidic extracellular gelling polysaccharide produced by *Pseudomonas elodea. Carbohydr. Res.* **124**, 123–133 (1983).

10. R. Chandrasekaran, R. P. Millane, S. Arnott, E. D. Atkins, The crystal structure of gellan. *Carbohydr. Res.* **175**, 1–15 (1988).

11. R. Chandrasekaran, L. C. Puigjaner, K. L. Joyce, S. Arnott, Cation interactions in gellan: An x-ray study of the potassium salt. *Carbohydr. Res.* **181**, 23–40 (1988).

12. E. Miyoshi, T. Takaya, K. Nishinari, Gel–sol transition in gellan gum solutions. II. DSC studies on the effects of salts. *Food Hydrocoll.* **8**, 529–542 (1994).

13. H. Moritaka, K. Nishinari, N. Nakahama, H. Fukuba, Effects of potassium chloride and sodium chloride on the thermal properties of gellan gum gels. *Biosci. Biotechnol. Biochem.* **56**, 595–599 (1992).

14. M. Watase, K. Nishinari, Effect of potassium ions on the rheological and thermal properties of gellan gum gels. *Food Hydrocoll.* **7**, 449–456 (1993).

15. E. Miyoshi, T. Takaya, K. Nishinari, Rheological and thermal studies of gel-sol transition in gellan gum aqueous solutions. *Carbohydr. Polym.* **30**, 109–119 (1996).

16. S. J. Pérez-Campos, N. Chavarría-Hernández, A. Tecante, M. Ramírez-Gilly, A. I. Rodríguez-Hernández, Gelation and microstructure of dilute gellan solutions with calcium ions. *Food Hydrocoll.* **28**, 291–300 (2012).

17. J. Tang, M. A. Tung, Y. Zeng, Gelling properties of gellan solutions containing monovalent and divalent cations. *J. Food Sci.* **62**, 688–712 (1997).

18. R. Mao, J. Tang, B. G. Swanson, Water holding capacity and microstructure of gellan gels. *Carbohydr. Polym.* **46**, 365–371 (2001).

19. H. Grasdalen, O. Smidsrød, Gelation of gellan gum. *Carbohydr. Polym.* **7**, 371–393 (1987).

20. T. Funami, S. Noda, M. Nakauma, S. Ishihara, R. Takahashi, S. Al-Assaf, S. Ikeda, K. Nishinari, G. O. Phillips, Molecular structures of gellan gum imaged with atomic force microscopy (AFM) in relation to the rheological behavior in aqueous systems in the presence of sodium chloride. *Food Hydrocoll.* **23**, 548–554 (2009).

21. C. Mazzuca, L. Micheli, M. Carbone, F. Basoli, E. Cervelli, S. Iannuccelli, S. Sotgiu, A. Palleschi, Gellan hydrogel as a powerful tool in paper cleaning process: A detailed study. *J. Colloid Interface Sci.* **416**, 205–211 (2014).

22. B. Di Napoli, S. Franco, L. Severini, M. Tumiati, E. Buratti, M. Titubante, V. Nigro, N. Gnan, L. Micheli, B. Ruzicka, C. Mazzuca, R. Angelini, M. Missori, E. Zaccarelli, Gellan gum microgels as effective agents for a rapid cleaning of paper. *ACS Appl. Polym. Mater.* **2**, 2791–2801 (2020).

23. A. M. Conte, O. Pulci, A. Knapik, J. Bagniuk, R. Del Sole, J. Lojewska, M. Missori, Role of cellulose oxidation in the yellowing of ancient paper. *Phys. Rev. Lett.* **108**, 158301 (2012).

24. C. Corsaro, D. Mallamace, J. Łojewska, F. Mallamace, L. Pietronero, M. Missori, Molecular degradation of ancient documents revealed by ${}^1$H HR-MAS NMR spectroscopy. *Sci. Rep.* **3**, 2896 (2013).

25. M. Missori, A. M. Conte, O. Pulci, L. Teodonio, S. Dominijanni, S. Puteo, S. Iannuccelli, S. Sotgiu, M. Sebastiani, Non-destructive monitoring of molecular modifications in the restoration of works of art on paper. *Eur. Phys. J. Plus* **134**, 99 (2019).

26. M. Caggioni, P. Spicer, D. Blair, S. Lindberg, D. Weitz, Rheology and microrheology of a microstructured fluid: The gellan gum case. *J. Rheol.* **51**, 851–865 (2007).

27. E. R. Morris, K. Nishinari, M. Rinaudo, Gelation of gellan–a review. *Food Hydrocoll.* **28**, 373–411 (2012).

28. V. Y. Grinberg, T. V. Burova, N. V. Grinberg, A. Y. Mashkevich, I. G. Plashchina, A. I. Usov, N. P. Shusharina, A. R. Khokhlov, L. Navarini, A. Cesàro, Thermodynamics of the double helix-coil equilibrium in tetramethylammonium gellan: High-sensitivity differential scanning calorimetry data. *Macromol. Biosci.* **3**, 169–178 (2003).

29. M. Diener, J. Adamcik, A. Sánchez-Ferrer, F. Jaedig, L. Schefer, R. Mezzenga, Primary, secondary, tertiary and quaternary structure levels in linear polysaccharides: From random coil, to single helix to supramolecular assembly. *Biomacromolecules* **20**, 1731–1739 (2019).

30. M. Diener, J. Adamcik, J. Bergfreund, S. Catalini, P. Fischer, R. Mezzenga, Rigid, fibrillar quaternary structures induced by divalent ions in a carboxylated linear polysaccharide. *ACS Macro Lett.* **9**, 115–121 (2020).

31. L. Schefer, J. Adamcik, R. Mezzenga, Unravelling secondary structure changes on individual anionic polysaccharide chains by atomic force microscopy. *Angew. Chem. Int. Ed.* **53**, 5376–5379 (2014).

32. L. Schefer, I. Usov, R. Mezzenga, Anomalous stiffening and ion-induced coil–helix transition of carrageenans under monovalent salt conditions. *Biomacromolecules* **16**, 985–991 (2015).

33. L. Schefer, J. Adamcik, M. Diener, R. Mezzenga, Supramolecular chiral self-assembly and supercoiling behavior of carrageenans at varying salt conditions. *Nanoscale* **7**, 16182–16188 (2015).

34. A. Gunning, V. J. Morris, Light scattering studies of tetramethyl ammonium gellan. *Int. J. Biol. Macromol.* **12**, 338–341 (1990).

35. G. Robinson, C. E. Manning, E. R. Morris, Conformation and physical properties of the bacterial polysaccharides gellan, welan, and rhamsan, in *Food Polymers, Gels and Colloids* (Woodhead Publishing, 1991), pp. 22–33.

36. T. Jamil, J. R. Gissinger, A. Garley, N. Saikia, A. K. Upadhyay, H. Heinz, Dynamics of carbohydrate strands in water and interactions with clay minerals: Influence of pH, surface chemistry, and electrolytes. *Nanoscale* **11**, 11183–11194 (2019).

37. O. Guvench, S. N. Greene, G. Kamath, J. W. Brady, R. M. Venable, R. W. Pastor, A. D. Mackerell Jr., Additive empirical force field for hexopyranose monosaccharides. *J. Comput. Chem.* **29**, 2543–2564 (2008).

38. C. Cencetti, D. Bellini, C. Longinotti, A. Martinelli, P. Matricardi, Preparation and characterization of a new gellan gum and sulphated hyaluronic acid hydrogel designed for epidural scar prevention. *J. Mater. Sci. Mater. Med.* **22**, 263–271 (2011).

39. R. Takahashi, H. Tokunou, K. Kubota, E. Ogawa, T. Oida, T. Kawase, K. Nishinari, Solution properties of gellan gum: Change in chain stiffness between single-and double-stranded chains. *Biomacromolecules* **5**, 516–523 (2004).

40. V. L. Larwood, B. J. Howlin, G. A. Webb, Solvation effects on the conformational behaviour of gellan and calcium ion binding to gellan double helices. *J. Mol. Model.* **2**, 175–182 (1996).

41. M. J. Frisch, G. W. Trucks, H. B. Schlegel, G. E. Scuseria, M. A. Robb, J. R. Cheeseman, G. Scalmani, V. Barone, G. A. Petersson, H. Nakatsuji, X. Li, M. Caricato, A. V. Marenich, J. Bloino, B. G. Janesko, R. Gomperts, B. Mennucci, H. P. Hratchian, J. V. Ortiz, A. F. Izmaylov, J. L. Sonnenberg, D. Williams-Young, F. Ding, F. Lipparini, F. Egidi, J. Goings, B. Peng, A. Petrone, T. Henderson, D. Ranasinghe, V. G. Zakrzewski, J. Gao, N. Rega, G. Zheng, W. Liang, M. Hada, M. Ehara, K. Toyota, R. Fukuda, J. Hasegawa, M. Ishida, T. Nakajima, Y. Honda, O. Kitao, H. Nakai, T. Vreven, K. Throssell, J. A. Montgomery Jr., J. E. Peralta, F. Ogliaro, M. J. Bearpark, J. J. Heyd, E. N. Brothers, K. N. Kudin, V. N. Staroverov, T. A. Keith, R. Kobayashi, J. Normand, K. Raghavachari, A. P. Rendell, J. C. Burant, S. S. Iyengar, J. Tomasi, M. Cossi, J. M. Millam, M. Klene, C. Adamo, R. Cammi, J. W. Ochterski, R. L. Martin, K. Morokuma, O. Farkas, J. B. Foresman, D. J. Fox, "Gaussian16 Revision C.01" (Gaussian Inc., 2016).

42. C. I. Bayly, P. Cieplak, W. Cornell, P. A. Kollman, A well-behaved electrostatic potential based method using charge restraints for deriving atomic charges: The RESP model. *J. Phys. Chem.* **97**, 10269–10280 (1993).

43. W. L. Jorgensen, J. Chandrasekhar, J. D. Madura, R. W. Impey, M. L. Klein, Comparison of simple potential functions for simulating liquid water. *J. Chem. Phys.* **79**, 926–935 (1983).

44. Y. Huang, N. Yang, Y. Zhang, J. Hou, Y. Gao, L. Tian, Z. Jin, Y. Shen, S. Guo, The gelling behavior of gellan in the presence of different sodium salts. *Int. J. Biol. Macromol.* **193**, 768–777 (2021).

45. R. W. Hockney, The potential calculation and some applications. *Methods Comput. Phys.* **9**, 136 (1970).

46. B. Hess, H. Bekker, H. J. Berendsen, J. G. Fraaije, Lincs: A linear constraint solver for molecular simulations. *J. Comput. Chem.* **18**, 1463–1472 (1997).

47. G. Bussi, D. Donadio, M. Parrinello, Canonical sampling through velocity rescaling. *J. Chem. Phys.* **126**, 014101 (2007).

48. H. J. C. Berendsen, J. P. M. Postma, W. F. van Gunsteren, A. DiNola, J. R. Haak, Molecular dynamics with coupling to an external bath. *J. Chem. Phys.* **81**, 3684–3690 (1984).

49. M. Parrinello, A. Rahman, Polymorphic transitions in single crystals: A new molecular dynamics method. *J. Appl. Phys.* **52**, 7182–7190 (1981).

50. S. Nosé, M. L. Klein, Constant pressure molecular dynamics for molecular systems. *Mol. Phys.* **50**, 1055–1076 (1983).

51. U. Essmann, L. Perera, M. L. Berkowitz, T. Darden, H. Lee, L. G. Pedersen, A smooth particle mesh Ewald method. *J. Chem. Phys.* **103**, 8577–8593 (1995).

52. M. J. Abraham, T. Murtola, R. Schulz, S. Páll, J. C. Smith, B. Hess, E. Lindahl, Gromacs: High performance molecular simulations through multi-level parallelism from laptops to supercomputers. *SoftwareX* **1-2**, 19–25 (2015).

53. S. Markidis, E. Laure, *Solving Software Challenges for Exascale: International Conference on Exascale Applications and Software, EASC 2014, Stockholm, Sweden, 2 to 3 April 2014 revised selected papers* (Lecture Notes in Computer Science (including subseries Lecture Notes in Artificial Intelligence and Lecture Notes in Bioinformatics), Springer, 2015), vol. 8759.

# Science Advances

## Molecular origin of the two-step mechanism of gellan aggregation

Letizia Tavagnacco, Ester Chiessi, Leonardo Severini, Silvia Franco, Elena Buratti, Angela Capocefalo, Francesco Brasili, Adriano Mosca Conte, Mauro Missori, Roberta Angelini, Simona Sennato, Claudia Mazzuca, and Emanuela Zaccarelli

**View the article online**
https://www.science.org/doi/10.1126/sciadv.adg4392
**Permissions**
https://www.science.org/help/reprints-and-permissions

Use of this article is subject to the Terms of service